HHS Public Access

Author manuscript

Nat Med. Author manuscript; available in PMC 2012 August 01.

Published in final edited form as:

Nat Med. ; 18(2): 302–306. doi:10.1038/nm.2615.

Magnetic Resonance Imaging of Glutamate

Kejia Cai[1,**], **Mohammad Haris**[1,**], **Anup Singh**[1,**], **Feliks Kogan**[1], **Joel H. Greenberg**[2], **Hari Hariharan**[1], **John A. Detre**[1,2,3], and **Ravinder Reddy**[1]

[1]CMROI, Department of Radiology, University of Pennsylvania, Philadelphia, PA, USA

[2]Department of Neurology, University of Pennsylvania, Philadelphia, PA, USA

[3]Center for Functional Neuroimaging, Department of Radiology, University of Pennsylvania, Philadelphia, PA, USA

Abstract

Glutamate (Glu) exhibits a pH and concentration dependent chemical exchange saturation transfer effect (CEST) between its -amine group and bulk water, here termed GluCEST. GluCEST asymmetry is observed at ~3 parts per million downfield from bulk water. Following middle cerebral artery occlusion in the rat brain, an approximately 100% elevation of GluCEST in the ipsilateral side compared to the contralateral side was observed, and is predominantly due to pH changes. In a rat brain tumor model with blood brain barrier disruption, intravenous Glu injection resulted in a clear elevation of GluCEST and a comparable increase in the proton magnetic resonance spectroscopy signal of Glu. GluCEST maps from healthy human brain at 7T were also obtained. These results demonstrate the feasibility and potential of GluCEST for mapping relative changes in Glu concentration as well as pH *in vivo*. Potential contributions from other brain metabolites to the GluCEST effect are also discussed.

INTRODUCTION

Glutamate (Glu) and gamma-aminobutyric acid (GABA) are the major excitatory and inhibitory neurotransmitters in the brain, respectively, and are likely involved in nearly all signal processing functions of the central nervous system (CNS) as well as being altered in many CNS diseases[1–4]. Magnetic resonance imaging (MRI) is a noninvasive imaging technique that provides exquisite structural detail, but current MRI methods are not capable of imaging the distribution of neurotransmitters in brain.

Address for Correspondence Ravinder Reddy, PhD, Center for Magnetic Resonance and Optical Imaging (CMROI), Department of Radiology, University of Pennsylvania, B1 Stellar-Chance Laboratories, 422 Curie Boulevard, Philadelphia, PA 19104-6100, Tel: (215) 898-5708, Fax: (215) 573-2113, ravi@mail.mmrrcc.upenn.edu.

**K.C., M.H., and A.S. share the equal authorship in the manuscript.

Author Contribution

K. C., M. H. and A. S. designed and performed experiments, analyzed data and wrote the manuscript; F. K. performed experiments and helped with manuscript editing; J. H. G. helped with animal studies and with manuscript editing; J. A. D. advised on neuroimaging aspects and contributed to the manuscript editing; H. H. provided pulse sequence design, technical guidance, and contributed to the manuscript writing; R. R. provided conception, overall experimental design and contributed to manuscript writing and editing.

Proton Magnetic Resonance Spectroscopy (^{1}HMRS) can detect several neurotransmitter signature groups using a variety of techniques [5–10].However, ^{1}HMRS techniques require long acquisition times and have poor spatial resolution. Here we describe a novel MRI technique for imaging Glu (*Unpublished results; R.R., K.C., M.H., A.S., F.K., H.H., Invention disclosure, University of Pennsylvania, Philadelphia, PA, September 3, 2009*) based on its chemical exchange saturation transfer (CEST)[11–15] effect (GluCEST) that provides markedly increased spatial and temporal resolution than ^{1}HMRS. The CEST effect from amide and hydroxyl protons from different amino acids, proteins and other molecules[12,16,17] have previously been exploited to measure pH *in vivo*[18,19], glycogen in the liver[20], glycosaminoglycans in cartilage[21], gene expression *in vivo*[22], and myo-inositol in brain,[23] but no prior studies have used the CEST effect of amineprotons to image Glu *in vivo*.

In the current study, the pH and concentration dependence of GluCEST is first demonstrated *in vitro* at 37 °C. Second, the feasibility of measuring GluCEST *in vivo* from rat brain with and without focal ischemia is shown. Third, changes in GluCEST and Glu ^{1}HMRS in response to exogenous injection of Glu in a rat brain tumor model are compared. Finally, the feasibility of mapping the Glu signal from healthy human brain *in vivo* is demonstrated at 7T. The potential contributions to GluCEST from other brain metabolites as well as the advantages and shortcomings of this approach are also discussed.

RESULTS

Phantom Studies

The z-spectra of 10 mM Glu at varying pH demonstrate that at lower pH (< pH 6.0), the CEST peak of Glu is sharper and centered around 3 parts per million (p.p.m.) downfield to the bulk water resonance (absolute chemical shift 7.7 p.p.m.) (Fig.1a). The z-spectral asymmetry plots (Fig.1b) exhibit a broad CEST effect ranging from 1 to 4 p.p.m. from bulk water resonance. While the GluCEST asymmetry plots from low pH solutions demonstrate clear peaks centered at ~3.00 p.p.m., the peak position of asymmetry plots from higher pH solutions (~6.0) gradually moved higher field towards water resonance. At pH 7, the maximum of asymmetry plot occurred at ~1.2 p.p.m. and its amplitude is ~100% higher than at 3 p.p.m.. This is a well-known phenomenon of intermediate to fast exchange ($k \leq \Delta\omega$) mediated chemical shift averaging. Despite the shift in peak position at pH 7, all studies reported in this work still use 3 p.p.m. as the GluCEST resonance saturation frequency to maintain consistency.

Due to non steady-state experimental conditions, the sensitivity of GluCEST was analyzed by solving numerical simulations of full Bloch-McConnell equations[24] using the experimental parameters from these studies. We found an excellent agreement between the experimental z-spectral asymmetry curves and numerically simulated ones. Since the intracellular pH (pHi) in the brain of normal healthy volunteers is reported to be around 7.0[25], the GluCEST contrast at this pH is the most relevant for *in vivo* imaging. Based on the fitted z-spectral asymmetry curve from simulations (Fig. 1b), the amine proton exchange rate (k) in a 10 mM Glu (pH 7.0) solution at 37°C was estimated to be in the range of 5,500 ± 500 s^{-1}. Since this is of the order of the chemical shift difference ($\Delta\omega$) at 7T ($\Delta\omega$=

5,700rad s^{-1}), GluCEST imaging is feasible at 7T as well as at higher fields. For the experimental saturation parameters used in this study, GluCEST increased gradually from pH 3 to pH 6 and then sharply decreased from pH 6 to 8. The largest GluCEST observed at pH 6 is likely due to the estimated reduced exchange rate of amine protons with the bulk water. GluCEST varies linearly with pH in the physiological range (6.0–7.4) (Fig. 1c).

There is a ~700 fold sensitivity advantage of GluCEST over conventional ^{1}HMRS at physiological concentration and temperature (Fig.1d–g). This sensitivity amplification should make it feasible to detect relatively small changes in Glu levels at high resolution (voxel size of 0.02 cc).

The GluCEST effect is linearly proportional to the Glu concentration ([Glu]) in the physiological range at pH 7 (Fig. 2a). With the imaging parameters used here, a ~0.6% CEST effect increase mM^{-1} [Glu] was observed (Fig. 2b). The GluCEST effect increased with peak B_1 amplitude and saturation pulse duration demonstrating that it is possible to obtain higher GluCEST effects (> 1% mM^{-1}) (Fig. 2c).

While it is possible to achieve a higher GluCEST sensitivity, in this study, the imaging parameters chosen were constrained by the exchange rate differences in phantoms and *in vivo* tissue as well as radio frequency (RF) specific absorption rate (SAR) issues dealing with human studies at 7T.

Potential Contributions From Other Brain Metabolites

The major metabolites in the brain visible with ^{1}HMRS at physiological concentrations are: N-acetyl aspartate (NAA), choline (Cho), myo-inositol (MI), creatine (Cr), glutamine (Gln), taurine, aspartate (Asp), Glu and GABA. After investigating the CEST properties each of these metabolites in phantoms, it was found that, with the experimental parameters used in this study, except for a small contribution from GABA and Cr, all other metabolites contribute negligible CEST effects to GluCEST (Fig. 2d,e). Of these metabolites, NAA has an amide proton and at neutral pH it does not exhibit any CEST effect. Cho does not have any exchangeable protons. MI has exchangeable –OH protons and exhibits a CEST effect at ≤ 1 p.p.m., which does not extend beyond 2 p.p.m. at neutral pH. Cr has amine protons that exhibit a CEST effect around 1.8 p.p.m. at physiological pH. However, its contribution to the GluCEST effect at 3 p.p.m. is also not appreciable (< 0.5%). No contributions to GluCEST were observed from Asp, Gln and taurine at their physiological concentrations under the experimental conditions used, possibly due to unfavorable exchange rates and differences in the chemical shifts of their amine protons.

Animal Studies

In the healthy rat brain, the gray matter (GM) and white matter (WM) are clearly separated in the GluCEST with a contrast ratio of ~1.6 (Fig. 3a–d). The Glu amine exchange rate measured in healthy rat brain was about 2,000 ± 500 s^{-1} (Supplementary Notes), which is well within the slow to intermediate exchange regime at 7T.

GluCEST obtained from a rat brain following middle cerebral artery occlusion (MCAO) stroke shows significant differences between ipsilateral and contralateral sides (Fig. 3e–h).

The ipsilateral side demonstrated a ~100% increase in GluCEST at 4.5 h after MCAO (Fig. 3h). The z-spectral asymmetry plots from the MCAO brain in the current study exhibit an elevation of CEST, whereas the z-spectra from a previously reported[18] MCAO study in the rat brain showed decreased amide proton CEST (APT) effects from the ipsilateral side compared to the contralateral side (Fig. 3i,j). Also, APT asymmetry plots show negative values at 3 p.p.m. whereas GluCEST shows positive values. This is due to key differences in the APT and GluCEST experimental conditions. In APT, due to low exchange rates (~30 s^{-1}), a lower saturation pulse amplitude (B_{1rms} = 50 Hz (1.2 μT)) and longer duration (~6 s) were used compared to those used in the present study (B_{1rms} = 155 Hz (3.6 μT) and 1 s).

Literature studies reveal that in this model of ischemia, extracellular Glu levels (~1–2 μM basal value) [26] increase substantially to ~0.2 mM[27]. However, the total Glu concentration (extra- and intra cellular) may remain unaltered. In addition, although extracellular concentrations (in μM) of other molecules such as GABA, Asp, adenosine and taurine also increase[28], their concentration changes are too small to account for the observed GluCEST effects.

In the MCAO model, it is also well-established that the magnitude of pH decrease expected over a four hour period is ~0.5 units[18]. In addition to pH, other factors that potentially affect GluCEST during stroke are changes to the water content, water T_2, and magnetization transfer ratio (MTR). It has been reported that in the MCAO model, the T_2 of water is elevated by ~20–40%, MTR is reduced by ~20%, and total water content may be changed by ~2–4%[18,29]. These changes in T_2, MTR and water content are expected to account for only minor changes in GluCEST.

Previous studies of polypeptide solutions in PBS have shown that the CEST effect from amine and amide protons decreased with decreasing pH in the range 7.3–5.0[30]. In contrast, GluCEST increased by almost 100% during MCAO ischemia in the present study. This increase in GluCEST is consistent with the pH dependent GluCEST behavior observed in Glu phantoms at physiological concentrations and temperature and suggests that the elevated GluCEST in the ipsilateral side of MCAO model is predominantly due to decreased pH.

In healthy brain, Glu does not cross the blood brain barrier (BBB), however the compromised BBB in a tumor model provides a means of demonstrating Glu modulation, where GluCEST should change approximately linearly with [Glu]. To demonstrate that the GluCEST measured *in vivo* is specific to Glu, GluCEST and ^{1}HMRS studies were performed in a rat brain with a tumor following the intravenous injection of Glu solution (Fig. 4a–f). GluCEST maps obtained at three time points after injection show that there is a significant increase in GluCEST in the tumor with a concomitant comparable elevation in the ^{1}HMRS of Glu.

In vivo Human Brain Study

A GluCEST map obtained from a healthy human brain (Fig. 5b) demonstrates a similar GM and WM distribution pattern as compared to a published Positron Emission Tomography (PET) map of the metabotropic Glu receptor subtype 5 (mGluR5) (Fig. 5c)[31]. Measured

[Glu] from the ^{1}HMRS data [WM = 5.9 ± 0.5 mM and GM = 9.4 ± 1.4 mM] are also consistent with the GluCEST from the same regions of interest (ROI) (Fig. 5a,b,f).

In human brain, the GM and WM GluCEST contrast is the highest at a saturation pulse length of ~1 s (Fig. 5g). The z-spectra and CEST asymmetry curves from GM and WM regions of the brain are rather broad and show a maximum CEST contrast at around 2 p.p.m. (Fig. 5i,j). The broadness in asymmetry plots may be partly due to the (i) broad asymmetry of Glu and the chemical shift averaging effect that shifts the line to higher field towards water resonance, and (ii) an additional potential contribution from creatine[32]. Similar results were observed from three volunteers. The intra-subject coefficient of variation of measured GluCEST was less than 5%.

The GluCEST maps obtained in healthy human brain reflect the known regional variation of physiological concentrations of glutamate[33,34]. Since ^{1}HMRS data is highly specific to [Glu], the observed strong correlation between GluCEST ratio from GM and WM ROIs (1.6 ± 0.2) with the measured [Glu] ratio from ^{1}H MRS data from the same ROIs (1.6 ± 0.1) provides additional confirmation that the observed GluCEST in the human brain is predominantly due to Glu. We estimate that ~70–75% of the observed GluCEST is from Glu (Supplementary Table 1 and Supplementary notes).

DISCUSSION

These findings provide the first evidence that GluCEST can be used to provide noninvasive images of [Glu] with excellent spatial and temporal resolution. In addition to its role as the predominant excitatory neurotransmitter in the brain, glutamate also serves as a metabolic intermediate, and it is likely that GluCEST detects both of these pools.

Although the GM to WM GluCEST contrast ratio in humans as well as in healthy rat brains is very similar (~1.6 ± 0.2), the GluCEST magnitude in the rat brain is higher than that in the human brain due to: (1) Higher field (9.4T *vs*. 7T), 2) continuous saturation pulses (constrained by the scanner software) and 3) lower direct water saturation at 9.4T compared to 7T. Due to the fast exchange rate of Glu amine protons, the slow to intermediate exchange rate condition is not fulfilled at 3T and hence these studies are expected to have poor sensitivity at 3T.

Potential contributions of MTR asymmetry to GluCEST, due to bound pool of water from rigid macromolecules in biological tissues, cannot be excluded. MTR asymmetry effect[35], if any, would compete with the GluCEST effect, and would lead to an underestimation of actual GluCEST levels. Indeed, the simulated MTR asymmetry (−0.14% in GM and −0.22% WM) (Supplementary Table 1) indicates that its contribution to the observed GluCEST is likely negligibly small.

In this study, SAR issues at 7T limit the observed GluCEST sensitivity in humans. However saturation pulse power, duration, pulse shapes and readout sequences in conjunction with multi-channel RF coils could be further optimized to enhance GluCEST effects within FDA guidelines for SAR deposition. The Glu contribution to GluCEST may have slight variations

per site depending on the RF coil or static field strength used, and future work should evaluate these contributions for specific experimental conditions.

Studies at ultrahigh fields beyond 7T would further enhance the sensitivity of GluCEST, albeit with additional challenges in dealing with SAR deposition. For proof of principle purposes, the current study used only a single slice with a two-dimensional imaging sequence. However, it would be relatively straightforward to implement a three dimensional acquisition of GluCEST maps.

In summary, GluCEST detection is feasible in the human brain at ultra high field (7T) without exceeding the allowed limits on SAR. About 70–75% of the observed CEST is from Glu with the remaining 25–30% coming from Cr, GABA and other macromolecules. Despite small contamination from other molecules *in vivo*, the GluCEST method can be used to study relative changes in Glu via endogenous or exogenous Glu modulation *in vivo*. This method provides noninvasive, nonradioactive and high spatial and temporal resolution imaging of relative changes in Glu for use in both human subjects and preclinical models. Further, the exquisite sensitivity of GluCEST to changes in pH could potentially be used as a pH marker in evolving stroke and tumors. Future studies using this approach may provide new insights into Glu function and demonstrate its potential as a biomarker for the diagnosis and treatment of CNS disorders.

ONLINE METHODS

All the phantom and human MRI studies were performed in a 7 T Siemens whole body MRI scanner (Siemens Medical Systems, Malvern, PA, USA) using a circularly polarized RF coil. All phantoms were prepared in PBS and all the experiments were performed at 37°C. Animal experiments were performed in a 9.4 T Varian scanner (Agilent Technologies, Palo Alto, CA, USA).

Phantom Imaging

A new pulse sequence was written to use a frequency selective saturation pulse followed by a segmented RF spoiled gradient echo (GRE) readout sequence. The imaging parameters were: slice thickness = 10 mm, flip angle = 10 °, TR = 5.6 ms, TE = 2.7 ms, field of view (FOV) = 120 × 120 mm^2, matrix size = 192 × 192, with one saturation pulse and 64 segments acquired every 15 s. CEST images were collected using a saturation pulse at a B_{1rms} of 155 Hz (3.6 μT) and 2 s duration and frequencies from − 5 to + 5 p.p.m. in steps of 0.2 p.p.m..

Animal Experiments

All animal experiments were performed according to an approved University of Pennsylvania institutional animal care and use committee (IACUC) protocol. For healthy and MCAO studies Sprague-Dawley male rats (265–315 g) and for tumor model studies female Fisher rats (130–150 g) were used. Both MCAO and tumor models were prepared as described in the Supplementary Notes.

Animal Imaging and Spectroscopy

Healthy (n = 2), MCAO (n = 3) and tumor bearing rats (n = 3) were imaged using 35-mm diameter quadrature RF coil (m2m Imaging Corp., Cleveland, OH, USA). Animals were kept under anesthesia (1.5% isoflurane in 1 l min^{-1} oxygen) and kept warm with the warm air generated from a heater. Respiration and body temperature were monitored using a MRI compatible small animal monitor system (SA Instruments, Inc., Stony Brook, NY, USA). CEST imaging was performed using a frequency selective continuous wave saturation pulse followed by a segmented GRE readout sequence. The imaging parameters were: FOV = 35 × 35 mm^2, slice thickness = 2 mm, flip angle = 15°, TR = 6.2 ms, TE = 2.9 ms, matrix size = 128 × 128, number of averages = 2, with one saturation pulse and 32 segments acquired every 4 s. CEST images were collected using a 1 s long rectangular saturation pulse at B_{1rms} of 250 Hz (5.9 μT) at multiple frequencies in the range − 5 to + 5 p.p.m. with a step size of 0.2 p.p.m.. Data for B_1 and B_0 maps were also acquired. *In vivo* exchange rate in healthy rat brain at 9.4T was measured using a previously described method[14].

In tumor bearing rats, along with GluCEST data, water suppressed stimulated echo acquisition mode (STEAM) single voxel spectra were obtained with the following parameters: voxel size = 11 × 8 × 5 mm^3, spectral width = 4 kHz, Number of points = 2048, average = 128, TE = 8 ms, TR = 6 s.

After collecting the baseline CEST map and ^{1}HMRS, the animals were injected with 2.5 ml, 100 mM glutamate solution through the tail vein. CEST and ^{1}HMRS data were gathered periodically for about 2 h post injection.

Human Studies

The study was conducted under an approved Institutional Review Board protocol of the University of Pennsylvania. GluCEST imaging and z-spectrum acquisitions on human brain at 7T were performed on three normal volunteers (male, age: 27-35 years). Informed consent from each volunteer was obtained after explaining the study protocol. Brain CEST imaging was performed with the application of the same imaging protocol as described for the phantoms except a larger FOV = 240 × 240 mm^2, averages = 4 and matrix size = 128 × 128. Original CEST images and GluCEST contrast maps were corrected for B_0 and B_1 inhomogeneities (Supplementary Notes).

Water suppressed ^{1}HMRS were obtained from GM and WM regions using the standard point resolved spectroscopy (PRESS)[36] localization technique with the following parameters: voxel size = 10 × 40 × 10 mm^3, spectral width = 4 kHz, number of points = 2048, average = 100, TE = 16 ms, and TR = 3 s.

Data Processing

All image processing and data analysis was performed using in-house written programs in MATLAB (version 7.5, R2007b). Acquired images were corrected for B_0 and B_1 inhomogeneities and z-spectra were obtained from these images by plotting the normalized image intensity as a function of resonance offset of saturation pulse for each sample.

CEST contrast was calculated from the Equation [1][37]

$$CEST_{asym}(\Delta\omega)=\frac{M_{sat}(-\Delta\omega)-M_{sat}(\Delta\omega)}{M_{sat}(-\Delta\omega)} \quad [1]$$

where $M_{sat}(\pm\Delta\omega)$ are the magnetizations obtained with saturation at a '+' or '−' $\Delta\omega$ offset from the water resonance.

[1]HMRS spectra were fitted using non-linear least squares methods with Gaussian functions. Peak integrals were calculated and normalized with a non-water suppressed proton signal for calculating Glu concentrations *in vivo*.

Supplementary Material

Refer to Web version on PubMed Central for supplementary material.

Acknowledgments

We gratefully acknowledge stimulating discussions with R. N. Bryan, M. D. Schnall, J. D. Glickson and W. S. Englander. Our thanks are due to W. Liu and S. Pickup for their technical assistance in using the 9.4 T research scanners, W. R. T. Witschey for technical support, P. Waghray for experimental help and D. Reddy, K. Nath and T. Hiraki for help with animal models. This work was performed at an US National Institutes of Health supported resource with funding from P41RR02305.

References

1. Petroff OA. GABA and glutamate in the human brain. Neuroscientist. 2002; 8:562–573. [PubMed: 12467378]
2. Harrison PJ. Metabotropic glutamate receptor agonists for schizophrenia. Br J Psychiatry. 2008; 192:86–87. [PubMed: 18245019]
3. Paul IA, Skolnick P. Glutamate and depression: clinical and preclinical studies. Ann N Y Acad Sci. 2003; 1003:250–272. [PubMed: 14684451]
4. Chojnacka-Wojcik E, Klodzinska A, Pilc A. Glutamate receptor ligands as anxiolytics. Curr Opin Investig Drugs. 2001; 2:1112–1119.
5. Rothman DL, Petroff OA, Behar KL, Mattson RH. Localized 1H NMR measurements of gamma-aminobutyric acid in human brain in vivo. Proc Natl Acad Sci U S A. 1993; 90:5662–5666. [PubMed: 8516315]
6. Ryner LN, Sorenson JA, Thomas MA. 3D localized 2D NMR spectroscopy on an MRI scanner. J Magn Reson B. 1995; 107:126–137. [PubMed: 7599948]
7. Ryner LN, Sorenson JA, Thomas MA. Localized 2D J-resolved 1H MR spectroscopy: strong coupling effects in vitro and in vivo. Magn Reson Imaging. 1995; 13:853–869. [PubMed: 8544657]
8. Hurd R, et al. Measurement of brain glutamate using TE-averaged PRESS at 3T. Magn Reson Med. 2004; 51:435–440. [PubMed: 15004781]
9. Gottschalk M, Lamalle L, Segebarth C. Short-TE localised 1H MRS of the human brain at 3 T: quantification of the metabolite signals using two approaches to account for macromolecular signal contributions. NMR Biomed. 2008; 21:507–517. [PubMed: 17955570]
10. Petroff OA, Mattson RH, Rothman DL. Proton MRS: GABA and glutamate. Adv Neurol. 2000; 83:261–271. [PubMed: 10999208]
11. Forsen S, Hoffman RA. Study of moderately rapid chemical exchange reactions by means of nuclear magnetic double resonance. J Chem Phys. 1963; 39:2892–2901.

12. Ward KM, Aletras AH, Balaban RS. A new class of contrast agents for MRI based on proton chemical exchange dependent saturation transfer (CEST). J Magn Reson. 2000; 143:79–87. [PubMed: 10698648]
13. Sherry AD, Woods M. Chemical exchange saturation transfer contrast agents for magnetic resonance imaging. Annu Rev Biomed Eng. 2008; 10:391–411. [PubMed: 18647117]
14. Woessner DE, Zhang S, Merritt ME, Sherry AD. Numerical solution of the Bloch equations provides insights into the optimum design of PARACEST agents for MRI. Magn Reson Med. 2005; 53:790–799. [PubMed: 15799055]
15. Zhou J, van Zijl PC. Chemcial exchange saturation transfer imaging and spectroscopy. Prog NMR Spectrosc. 2006; 48:109–136.
16. Jones CK, et al. Amide proton transfer imaging of human brain tumors at 3T. Magn Reson Med. 2006; 56:585–592. [PubMed: 16892186]
17. Englander SW, Downer NW, Teitelbaum H. Hydrogen exchange. Annu Rev Biochem. 1972; 41:903–924. [PubMed: 4563445]
18. Zhou J, Payen JF, Wilson DA, Traystman RJ, van Zijl PC. Using the amide proton signals of intracellular proteins and peptides to detect pH effects in MRI. Nat Med. 2003; 9:1085–1090. [PubMed: 12872167]
19. Sun PZ, Zhou J, Sun W, Huang J, van Zijl PC. Detection of the ischemic penumbra using pH-weighted MRI. J Cereb Blood Flow Metab. 2007; 27:1129–1136. [PubMed: 17133226]
20. van Zijl PC, Jones CK, Ren J, Malloy CR, Sherry AD. MRI detection of glycogen in vivo by using chemical exchange saturation transfer imaging (glycoCEST). Proc Natl Acad Sci U S A. 2007; 104:4359–4364. [PubMed: 17360529]
21. Ling W, Regatte RR, Navon G, Jerschow A. Assessment of glycosaminoglycan concentration in vivo by chemical exchange-dependent saturation transfer (gagCEST). Proc Natl Acad Sci U S A. 2008; 105:2266–2270. [PubMed: 18268341]
22. Gilad AA, et al. Artificial reporter gene providing MRI contrast based on proton exchange. Nat Biotechnol. 2007; 25:217–219. [PubMed: 17259977]
23. Haris M, Cai K, Singh A, Hariharan H, Reddy R. In vivo mapping of brain myo-inositol. Neuroimage. 2010
24. McConnell HM. Reaction rates by nuclear magnetic resonance. J Chem Phys. 1958; 28:430–431.
25. Chu WJ, et al. Is the intracellular pH different from normal in the epileptic focus of patients with temporal lobe epilepsy? A 31P NMR study. Neurology. 1996; 47:756–760. [PubMed: 8797475]
26. Davalos A, Shuaib A, Wahlgren NG. Neurotransmitters and pathophysiology of stroke: evidence for the release of glutamate and other transmitters/mediators in animals and humans. J Stroke Cerebrovasc Dis. 2000; 9:2–8. [PubMed: 17895213]
27. Kiewert C, Mdzinarishvili A, Hartmann J, Bickel U, Klein J. Metabolic and transmitter changes in core and penumbra after middle cerebral artery occlusion in mice. Brain Res. 2010; 1312:101–107. [PubMed: 19961839]
28. Melani A, et al. Striatal outflow of adenosine, excitatory amino acids, gamma-aminobutyric acid, and taurine in awake freely moving rats after middle cerebral artery occlusion: correlations with neurological deficit and histopathological damage. Stroke. 1999; 30:2448–2454. discussion 2455. [PubMed: 10548683]
29. Tuor UI, et al. Differential progression of magnetization transfer imaging changes depending on severity of cerebral hypoxic-ischemic injury. J Cereb Blood Flow Metab. 2008; 28:1613–1623. [PubMed: 18506197]
30. McMahon MT, et al. New “multicolor” polypeptide diamagnetic chemical exchange saturation transfer (DIACEST) contrast agents for MRI. Magn Reson Med. 2008; 60:803–812. [PubMed: 18816830]
31. Ametamey SM, et al. Human PET studies of metabotropic glutamate receptor subtype 5 with 11C-ABP688. J Nucl Med. 2007; 48:247–252. [PubMed: 17268022]
32. Sun PZ, Sorensen AG. Imaging pH using the chemical exchange saturation transfer (CEST) MRI: Correction of concomitant RF irradiation effects to quantify CEST MRI for chemical exchange rate and pH. Magn Reson Med. 2008; 60:390–397. [PubMed: 18666128]

33. Michaelis T, Merboldt KD, Bruhn H, Hanicke W, Frahm J. Absolute concentrations of metabolites in the adult human brain in vivo: quantification of localized proton MR spectra. Radiology. 1993; 187:219–227. [PubMed: 8451417]

34. Choi IY, Lee SP, Merkle H, Shen J. In vivo detection of gray and white matter differences in GABA concentration in the human brain. Neuroimage. 2006; 33:85–93. [PubMed: 16884929]

35. Hua J, et al. Quantitative description of the asymmetry in magnetization transfer effects around the water resonance in the human brain. Magn Reson Med. 2007; 58:786–793. [PubMed: 17899597]

36. Bottomley PA. Spatial localization in NMR spectroscopy in vivo. Ann N Y Acad Sci. 1987; 508:333–348. [PubMed: 3326459]

37. Liu G, Gilad AA, Bulte JW, van Zijl PC, McMahon MT. High-throughput screening of chemical exchange saturation transfer MR contrast agents. Contrast Media Mol Imaging. 2010; 5:162–170. [PubMed: 20586030]

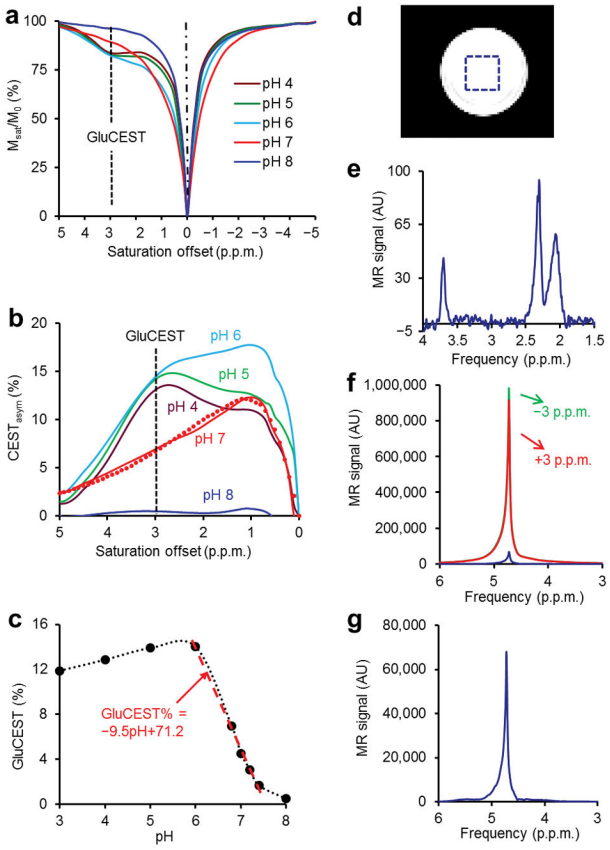

Figure 1.

pH dependence and sensitivity advantage of GluCEST. (**a**) CEST z-spectra of 10 mM Glu at varying pH and 37°C at 7T show the CEST effect at 3 p.p.m. downfield to bulk water resonance. (**b**) GluCEST asymmetry curves from different pH solutions corresponding to (**a**). The overlay of simulated GluCEST (dotted line) on the curve corresponding to pH 7 is also shown. (**c**) This plot shows dependence of GluCEST on pH (3–8). The fitted line shows linear dependence of GluCEST in physiological pH range (6.0–7.4). (**d**) Image from a phantom of 10 mM glutamate (pH = 7.0, 37°C) prepared in PBS with the localization voxel indicated. (**e**) ^{1}HMRS PRESS water suppressed spectrum (TR = 20 s, TE = 16 ms, 4 averages) from the single voxel shown in the image (**d**). The three resonances correspond to two –CH_2 groups and one –CH group of glutamate. (**f**) Water ^{1}H resonance spectra obtained while saturating at ± 3 p.p.m. as well as their difference spectrum. (**g**) The rescaled difference spectrum from (**f**). The difference spectrum represents the 3 p.p.m. point on the CEST asymmetry spectrum. The ratio of the CEST difference spectrum to Glu –CH_2 resonance at 2.3 p.p.m. is ~700.

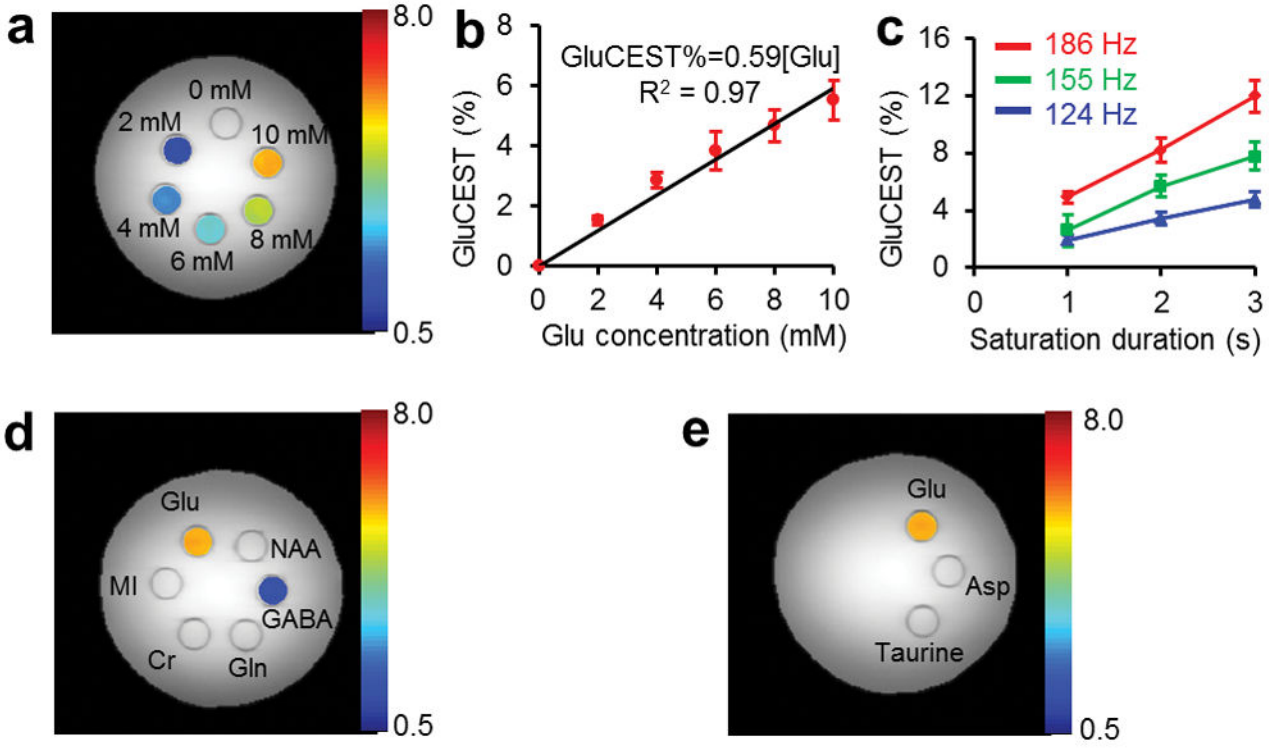

Figure 2.

GluCEST images at 7T of a phantom consisting of test tubes with different concentrations of Glu solutions (pH 7.0) immersed in a beaker containing PBS. All the experiments were performed at 37 °C (**a**) Shows the GluCEST contrast color-coded on the original CEST image (3 p.p.m.), acquired with application of saturation pulse train with B_{1rms} = 155 Hz (3.6 μT) for 2 s. Color bar represents GluCEST contrast in percentage. (**b**) Approximately linear dependence of GluCEST effect on Glu concentration with a slope of 0.6% mM^{-1} Glu. (**c**) GluCEST dependence on B_{1rms} and duration of the saturation pulse. **(d,e)** CEST images of a phantom consisting of test tubes with solution of different metabolites at their physiological concentrations and pH 7 [Glu (10 mM), GABA (2 mM), NAA (10 mM), Gln (2 mM), Asp (2 mM), taurine (2 mM), Cr (6 mM) and MI (10 mM)] immersed in a beaker containing PBS. The CEST contrast color-coded on the original CEST images (3 p.p.m.), which show the substantial CEST contrast from Glu (~6%), and ~1% from GABA, < 0.5% from Cr and no contrast from other metabolites. Color bar represents CEST contrast in percentage.

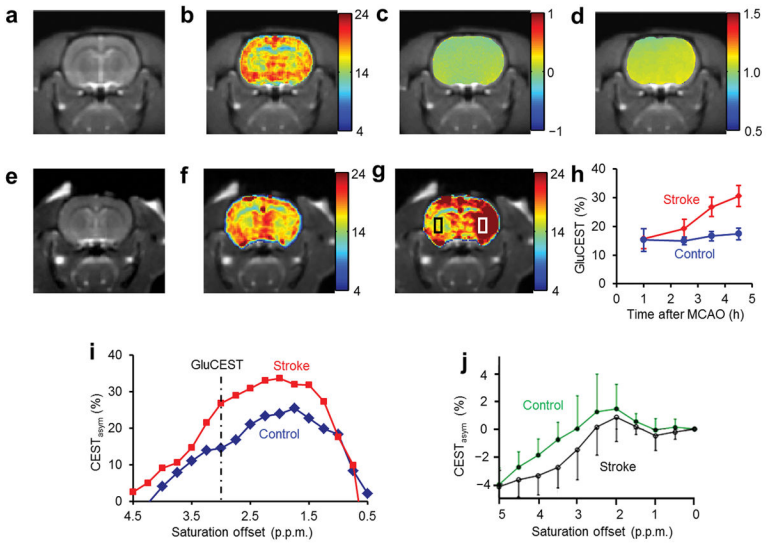

Figure 3.

GluCEST maps of healthy and ischemic rat brain. (**a**) Rat brain anatomic images, (**b**) GluCEST maps, (**c**) and (**d**) show B_0, and B_1 maps of the corresponding brain slices, respectively. Clear differences of GluCEST contrast in GM and WM regions can be seen. (**e**) Rat brain anatomic proton image. (**f,g**) The GluCEST maps of the rat brain acquired at 1 h and 4.5 h following the induction of stroke. (**h**) The GluCEST contrast vs. time after MCAO at regions of interest within the rectangular areas shown in (**g**). In the ipsilateral side GluCEST is almost doubled at 4.5 h after occlusion. (**i**) The GluCEST asymmetry plots from the contralateral side (blue curve) and ipsilateral side (red curve) at 4.5 h after occlusion. At 3.00 p.p.m., it is evident that there is almost 100% increase in GluCEST. (**j**) The contralateral and ipsilateral sides of MCAO rat brain data acquired at 4.7T after 4 h post occlusion and 1 h post mortem (Reprinted by permission from Macmillan Publishers Ltd: Nature Medicine [18], Figure 4, copyright (2003)).

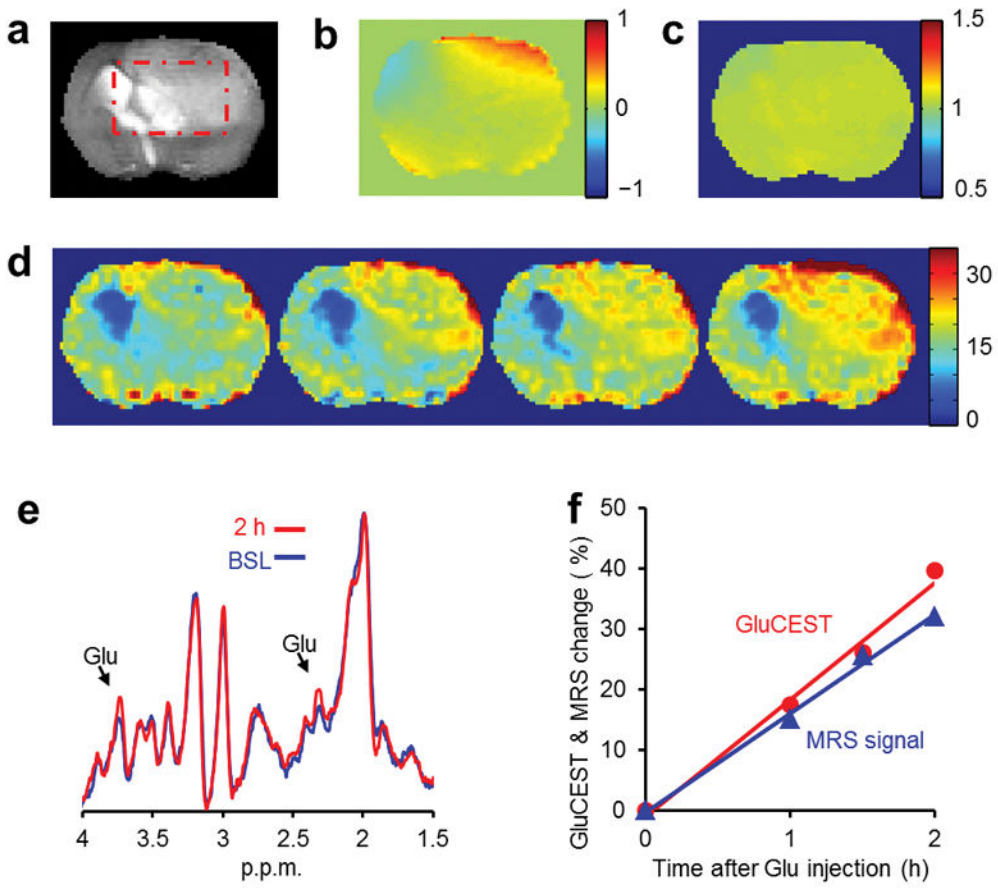

Figure 4.

GluCEST images and ^{1}HMRS of rat brain with tumor before and after injection of Glu. (**a**) Rat brain anatomic proton image demonstrating the tumor and a rectangular region of interest. (**b**) B_0 map of the rat brain, which shows about ± 0.5 p.p.m. variation. (**c**) B_1 map of the rat brain showing fairly uniform B_1 field. (**d**) GluCEST maps (color bar represents GluCEST contrast in percentage) of the rat brain acquired pre-injection (BSL) and at 1, 1.5 and 2.0 h following the injection of Glu solution. Gradual elevation in the GluCEST is evident over a period of 2 h. (**e**) Stacked stimulated echo acquisition mode (STEAM) localized ^{1}HMRS data acquired at baseline and at 2 h following the injection. Clear elevation of Glu $–CH_2$ (2.3 p.p.m.) and –CH peak (3.75 p.p.m.) amplitude can be seen in the spectra. (**f**). Time course of GluCEST and the 2.3 p.p.m. Glu peak integral normalized with the values of pre-injection from regions of interest within the rectangular areas shown in (**a**). A strong correlation between GluCEST and ^{1}HMRS data can be seen.

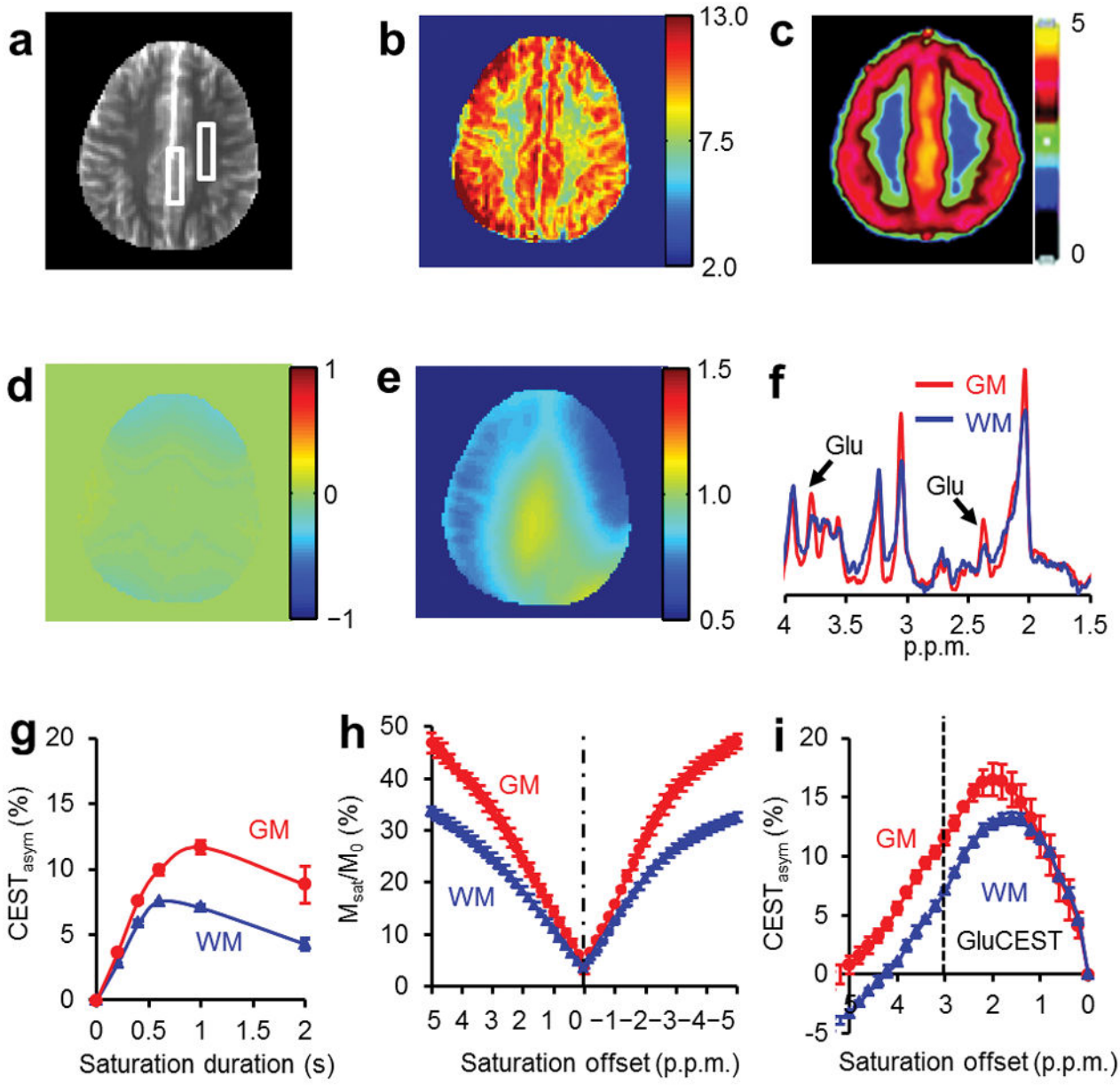

Figure 5.

GluCEST imaging and ^{1}HMRS from a healthy human brain acquired at 7T. (**a**) Anatomic proton image of the axial slice. (**b**) B_1 and B_0 corrected GluCEST contrast map (Color bar represents GluCEST contrast in percentage). (**c**) Map of distribution volumes (DVs) of metabotropic Glu receptor subtype 5 from a PET image *(Reprinted by permission of the Society of Nuclear Medicine: J Nucl Med* [31], Figure 2, copyright (2007)). The GluCEST map and the PET image show similar distribution pattern of Glu in brain, which is higher in GM compared to WM. (**d**) B_0 map and (**e**) B_1 map corresponding to the slice in (**a**). (**f**) ^{1}HMRS spectra obtained from regions of interest of GM and WM as shown in (**a**). These spectra show higher amplitude of Glu $–CH_2$ resonance (2.3 p.p.m.) and –CH resonance (3.75 p.p.m.) in GM than that in WM. (**g**) Saturation pulse duration dependence of GluCEST

data from human brain. The GluCEST reaches a maximum at a saturation duration of ~1 s and decreases with further increase in duration. (**h,i**) z-spectra and corresponding asymmetry plots from human GM and WM regions. The GluCEST at 3 p.p.m. (dotted line in figure **i**) is ~11% from GM and ~7% from WM.